The Journal of the Astronautical Sciences (2023) 70:24
https://doi.org/10.1007/s40295-023-00389-5

ORIGINAL ARTICLE

Construction of Heteroclinic Connections Between Quasi-Periodic Orbits in the Three-Body Problem

Brian McCarthy[1,2] · **Kathleen Howell**[1]

Accepted: 19 June 2023 / Published online: 20 July 2023

Abstract
Quasi-periodic orbits offer a broad range of flexibly and adaptable destinations in multi-body systems. In this investigation, a computational framework for construction of heteroclinic connections between quasi-periodic orbits is summarized. Subsequently, families of heteroclinic connections are characterized and examples are provided in the Circular Restricted Three-Body Problem (CR3BP). Transition to an ephemeris model is also demonstrated. An understanding of these types of transfers is crucial for a more complete picture of the flow in a three-body system.

Keywords Quasi-periodic orbits · Dynamical systems theory · Three-body problem · Heteroclinic connections

1 Introduction

In 2020, NASA released the agency's lunar exploration program overview, offering the status of Artemis and Gateway as well as plans for additional extended lunar missions [1]. Additionally, the Artemis 1 mission successfully tested the Orion capsule in deep space in 2022 [2]. To enable such endeavors, an understanding of the cislunar gravitational environment is crucial and essential to the success of these programs. However, given the chaotic nature of a multi-body system, preliminary path planning in this environment is challenging. To meet these challenges, streamlining the trajectory design process by leveraging dynamical structures in cislunar

Brian McCarthy and Kathleen Howell have contributed equally to this work.

✉ Brian McCarthy
brian.mccarthy@ai-solutions.com

Kathleen Howell
howell@purdue.edu

[1] School of Aeronautics and Astronautics, Purdue University, 701 W. Stadium Ave, West Lafayette, IN 47907, USA

[2] a.i. solutions, Inc, 2101 E NASA Pkwy, Houston, TX 77058, USA

space is enabling. In this investigation, a computational framework is developed to construct maneuver-free, heteroclinic transfers between quasi-periodic orbits (QPOs) in the CR3BP. Furthermore, quasi-periodic orbits expand the design space and add flexibility in orbit selection as well as the construction of transfer paths. Quasi-periodic orbit characterization and stability properties are initially summarized. Then, the process to produce initial guesses using Poincaré mapping is demonstrated. Finally, the computational algorithm to compute families of heteroclinic transfers is detailed and these families of solutions are characterized in the Earth-Moon CR3BP. Ultimately, the framework for this investigation augments the existing techniques for path planning in multi-body regimes.

Several authors have examined heteroclinic connections between quasi-periodic orbits previously. Calleja et al. demonstrate an indirect method to compute heteroclinic connections between periodic and quasi-periodic orbits using collocation [3]. Goméz focuses on connections using a large set of trajectories propagated from the semi-analytic center manifold [4]. Olikara expands upon both approaches in developing a boundary value problem to compute heteroclinic connections between quasi-periodic tori [5]. Most recently, Bonasara and Bosanac explore heteroclinic connections between quasi-periodic orbits near resonances by leveraging unsupervised machine learning techniques [6]. De Smet and Scheeres also investigate identification of heteroclinic connections using artificial neural networks [7]. Henry and Scheeres also surveyed the heteroclinic connections in the Earth-Moon system to traverse between L_1 and L_2 [8]. This investigation builds upon previous work by McCarthy and Howell to construct of heteroclinic connections between quasi-periodic orbits [9]. Specifically, the contribution of this investigation is the development of a unique framework to, first, find potential heteroclinic connections between QPOs, then compute families of heteroclinic transfers, and lastly, demonstrate that the transfers maintain their geometry when transitioned to a higher-fidelity ephemeris model. First, potential heteroclinic connections between quasi-periodic orbits are isolated by leveraging Poincaré maps. Then, families of connections are characterized and constructed by varying the destination orbit, the departing orbit, or the Jacobi Constant across each member of a family; examples of these families are constructed in the Earth-Moon system. Details of a targeting process to compute each member of the family are summarized; this summary includes addressing challenges associated with partial derivative calculations with higher-order finite differencing to improve targeter convergence behavior. Finally, the transition process to an ephemeris model leverages a mutliple shooting differential corrections algorithm to show that the geometry of solutions obtained in the Earth-Moon CR3BP exist in a higher-fidelity model that more accurately represents the space environment. The examples in this investigation seek to demonstrate the flexibility of the framework, highlight its usefulness within the multi-body trajectory design process, and provide an additional

set of tools to incorporate quasi-periodic orbits into the end-to-end trajectory design process.

2 Dynamical Model

The CR3BP offers higher fidelity and additional behaviors in comparison to the two-body model. In this multi-body model, two gravitational bodies, denoted P_1 and P_2, remain in circular Keplerian orbits about their mutual barycenter (i.e., center of mass). A third body, P_3, moves under the gravitational influence of the two larger bodies and is assumed to be massless. The model is defined relative to a rotating coordinate system, where the $+\hat{x}$ direction is defined from the barycenter toward P_2. The $+\hat{z}$ direction is defined parallel to the direction of the orbital angular momentum vector for P_1 and P_2; the $\hat{y}$ direction completes the orthonormal triad. The nondimensional position and velocity for P_3 relative to the barycenter in the rotating frame are defined as $\boldsymbol{x} = \left[x\ y\ z\ \dot{x}\ \dot{y}\ \dot{z}\right]^T$, where the first three and the last three elements are the position and relative velocity components, respectively. The equations of motion for a particle moving in the CR3BP are a set of three, second-order scalar differential equations of motion,

$$\ddot{x} - 2\dot{y} = \frac{\partial U^*}{\partial x} \quad \ddot{y} + 2\dot{x} = \frac{\partial U^*}{\partial y} \quad \ddot{z} = \frac{\partial U^*}{\partial z} \tag{1}$$

The pseudo-potential function is a scalar defined solely in terms of position and the CR3BP nondimensional mass parameter, $\mu = M_2/(M_1 + M_2)$, where M_1 and M_2 are the masses of P_1 and P_2, respectively [10]. The pseudo-potential function takes the following form,

$$U^* = \frac{x^2 + y^2}{2} + \frac{\mu}{r} + \frac{1-\mu}{d} \tag{2}$$

where $d = \sqrt{(x+\mu)^2 + y^2 + z^2}$ and $r = \sqrt{(x-1+\mu)^2 + y^2 + z^2}$ represent the nondimensional distances of P_3 relative to P_1 and P_2, respectively. The CR3BP admits a single integral of the motion, commonly denoted the Jacobi Constant (JC). The Jacobi Constant is a function of the pseudo-potential and the rotating velocity magnitude expressed in the rotating reference frame,

$$JC = 2U^* - v^2 \tag{3}$$

where $v = \sqrt{\dot{x}^2 + \dot{y}^2 + \dot{z}^2}$. The Jacobi Constant is an energy-like quantity that characterizes motion in a CR3BP system and remains constant for all time over any ballistic arc propagated in the CR3BP. One advantage of the CR3BP model is that the system is time invariant. The CR3BP is a good approximation for a multi-body environment and the trajectory characteristics generally persist when transitioning results to a higher-fidelity ephemeris model [11, 12].

3 Characteristics of Quasi-Periodic Orbits

Quasi-periodic orbits exist in the vicinity of periodic solutions when the monodromy matrix possesses complex eigenvalues of unit magnitude. Furthermore, quasi-periodic trajectorties are represented along families of invariant tori. Invariant tori are characterized by the number of fundamental frequencies that define the motion on the torus, such that an n-dimensional torus possesses n fundamental frequencies. Equilibrium solutions and periodic orbits are examples of 0-dimensional and 1-dimensional tori, respectively. For a periodic orbit, a single fundamental frequency defines the motion. Quasi-periodic orbits then evolve on tori where $n > 1$. In the CR3BP, 2-dimensional quasi-periodic tori are known to exist in two-parameter families [13]. The algorithm to compute QPO families is detailed by McCarthy and Howell; the basic framework was originally developed by Olikara and Scheeres, Castella and Jorba, as well as Gomez and Mondelo [13–16]. This algorithm was selected for this investigation based on the conclusions by Baresi, Olikara, and Scheeres on the runtime and accuracy of the algorithm [17]. In Fig. 1, members of three different quasi-vertical families are rendered in the Earth-Moon CR3BP; all originate from the same periodic vertical orbit. Each of these families possess a characteristic quantity that is constant across all members of an individual family. For example, the members in Fig. 1a all possess the same Jacobi Constant value and the members in Fig. 1c all possess the same frequency ratio. Additionally, linear stability is determined for quasi-periodic orbits by assessing the characteristics of the eigenstructure in the stroboscopic map, as summarized by Jorba, Olikara and Scheeres as well as McCarthy and Howell [13, 14, 18]. The linear stability is assessed through variations associated with the invariant curve of the QPO. A convenient stability index metric is defined by McCarthy and Howell, such that when the stability index is equal to unity, the QPO is considered stable, and when the stability index is greater than unity, the QPO is characterized as unstable [14]. Unstable orbits possess stable and unstable manifolds that asymptotically approach and depart the orbit, repsectively; these manifolds are the basis for the construction of the heteroclinic connections [3, 5, 8].

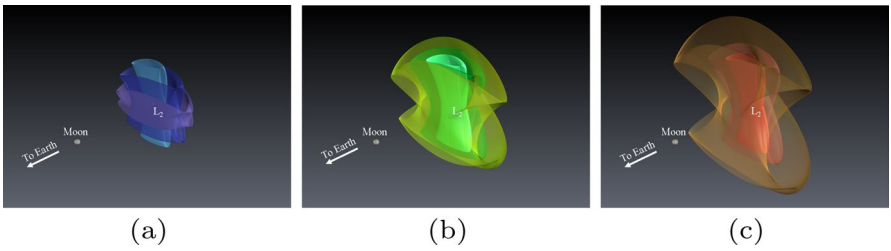

Fig. 1 Members of the L_1 quasi-vertical families where **a** Jacobi Constant is fixed for all members, **b** the stroboscopic mapping time is fixed for all members, and **c** the frequency ratio is fixed for all members in the Earth-Moon CR3BP

4 Heteroclinic Connections

Heteroclinic transfers within the context of astrodynamics are defined as paths that flow freely from a departing orbit to a destination orbit by means of stable and unstable manifold trajectories. A particle moving along an unstable manifold from the originating orbit simultaneously flows onto the stable manifold of the destination orbit, such that no maneuver impulse is required to change the path. These types of transfers are leveraged for trajectory design, and also provide a broader understanding of the flow within a given region of a multi-body space. This investigation is focused on the development of an effective strategy to construct and characterizes heteroclinic connections between quasi-periodic tori. Given the higher dimensionality of the spatial problem, as compared to the planar CR3BP, challenges exist in locating an initial heteroclinic connection between two orbits. A method developed by Haapala and Howell is expanded to leverage glyphs and produce an initial guess for a heteroclinic connection between two quasi-periodic orbits [19]. Next, a differential corrections procedure delivers a continuous heteroclinic connection between two orbits. Finally, a continuation process is leveraged to generate a family of heteroclinic connections.

4.1 Poincaré Mapping

Poincaré maps are a useful tool in the identification of solutions in the trajectory design problem. They reduce the dimensionality of the design space to expedite the process of initial guess construction for transfer trajectories. Maps are also augmented through the use of coloring or glyphs to represent additional information. Ponicaré maps are first constructed by selecting a hyperplane to examine the flow. In this investigation, the hyperplanes include a physical plane (i.e., the $\hat{x}\hat{z}$ plane in the rotating frame) as well as some characteristic of the path (i.e., a periapsis condition). To visually represent this technique, consider the hyperplane Σ in Fig. 2. Trajectories that pass through or satisfy the condition for the defined hyperplane along their path are recorded. Evolution of the states is observed between $\bar{x}_{R0}$ and $\bar{x}_{R1}$, as the trajectory moves forward in time. Additionally,

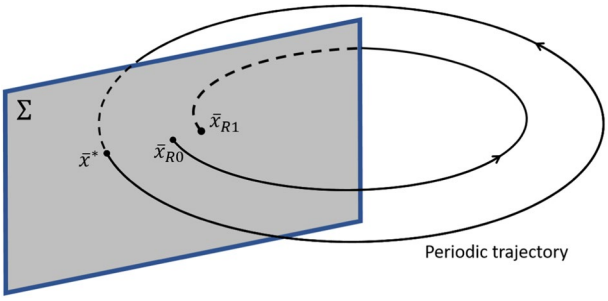

Fig. 2 Diagram of Poincaré mapping technique

trajectories that return to the same location on the map are considered periodic, exemplified by the state $\bar{x}^*$ on the hyperplane in Fig. 2. In this investigation, Poincaré maps aid in identifying potential heteroclinic transfers.

4.2 Identification of an Initial Guess

To determine an initial guess for a potential heteroclinic connection, information from Poincaré maps is leveraged to isolate candidate transfers. Consider two unstable QPOs in the Earth-Moon CR3BP, one unstable L_1 QPO and an L_2 unstable QPO. Both of these orbits are constructed such that their energy value is selected as $JC = 3.11$. Since both of these orbits exist at the same Jacobi Constant level, it is possible that heteroclinic connections exist that render maneuver-free paths between them. Trajectories representing the unstable manifolds are propagated in forward time from the L_2 quasi-halo orbit and recorded whenever they cross the $\hat{x}\hat{z}$ plane in the Earth-Moon rotating frame. Similarly, trajectories representing the stable manifolds of the L_1 quasi-halo are propagated in reverse time and the crossings are recorded. From the recorded states, a Poincaré map is created using the position and velocity information, where states from the stable and unstable manifolds are plotted in blue and red, respectively, in Fig. 3. The position at the crossing of the plane is recorded as a point and the velocity information is represented as an arrow. The direction of the arrow indicates the direction of the $\hat{x}$ and $\hat{z}$ components of velocity at the plane crossing, while the length of the arrow indicates the magnitude of each of the $\hat{x}$ and $\hat{z}$ velocity components. Lastly, only states with $\dot{y} > 0$ are rendered on the map so that the direction of the flow through the map is consistent between the stable and unstable trajectories. Thus, an initial guess is selected from the map such that two points that share a similar x- and z-position as well as possess arrows in nearly the same direction and magnitude. The process of selecting the stable and unstable connection initial guess is performed visually in Fig. 3, which is similar to the process leveraged by Haapala and Howell [19]. The initial guesses used to

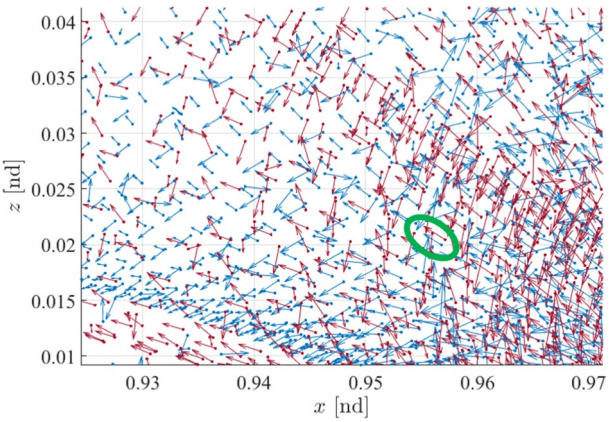

Fig. 3 Poincaré map with the stable manifold trajectory points (blue) from an L_1 quasi-halo orbit and the unstable manifold trajectory points (blue) from an L_2 quasi-halo orbit

construct Figs. 8 and 9a were selected by performing an all-to-all comparison of the stable and unstable information on the map, i.e., the norm of the difference between the x, z, $\dot{x}$, and $\dot{z}$ components of the stable and unstable manifold trajectories represented on the map is computed, and the trajectories associated with the lowest norm are considered as possible connections. While selecting a point using this criteria does not guarantee a connection, it supplies a sufficient initial guess to seed a differential corrections algorithm.

4.3 Targeting a Heteroclinic Connection

The targeting problem to compute heteroclinic connections is an extension of the formulation by Haapala and Howell in the CR3BP as well as McCarthy and Howell in the Bicircular Restricted Four-Body Problem [19, 20] and the scheme is illustrated in the diagram in Fig. 4. In Fig. 4, the red oval reflects the initial torus and the blue oval indicates the destination torus.

The states retrieved from the Poincaré map deliver the initial guess for the black path in Fig. 4. The constraint vector is then defined,

$$\boldsymbol{F} = \begin{bmatrix} \boldsymbol{F}_1 \\ \boldsymbol{F}_2 \end{bmatrix} = \begin{bmatrix} \boldsymbol{x}_T - \left(\boldsymbol{x}^t_{M,u} + d_u \frac{\Phi_u \boldsymbol{v}_u}{|\Phi_u \boldsymbol{v}_u|} \right) \\ \boldsymbol{x}^t_T - \left(\boldsymbol{x}^t_{M,s} + d_s \frac{\Phi_s \boldsymbol{v}_s}{|\Phi_s \boldsymbol{v}_s|} \right) \end{bmatrix} \tag{4}$$

where $\mathbf{x}_T$ is the originating state on the transfer segment and $\mathbf{x}^t_T$ reflects the state on the transfer segment after it is forward propagated for time T_T. Then, d_u and d_s are scalars that define the small perturbation of the state along the unstable and stable manifold directions, respectively; $\mathbf{v}_u$ and $\mathbf{v}_s$ are the 6×1 stable and unstable eigenvectors at latitudinal angles of $\theta_{1,u}$ and $\theta_{1,s}$, respectively, on the invariant curve for their respective orbits, and Φ_u and Φ_s are the state transition matrices propagated from their initial states for time τ_u and τ_s, respectively, $\mathbf{x}_{M,u}$ and $\mathbf{x}_{M,s}$, on the invariant curve for the initial and destination tori, respectively. Note that the values for d_s and d_u are equal to 0.0001 for all cases in this investigation. Also note that setting

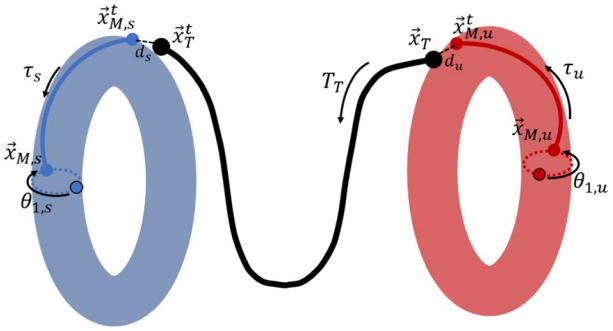

Fig. 4 Heteroclinic targeting procedure diagram

d_u and d_s equal to a larger number could cause the trajectories to no longer represent the manifolds, while smaller values for d_u and d_s could result in longer propagation times. The value chosen for this investigation intends to balance both trade-offs. Subsequently, a free variable vector is defined,

$$\boldsymbol{X} = \begin{bmatrix} \boldsymbol{x}_T & T_T & \tau_u & \tau_s & \theta_{1,u} & \theta_{1,s} \end{bmatrix}^T \tag{5}$$

where T_T is the time along the transfer segment, τ_u is the time from the invariant curve departure to the unstable perturbation location on the initial torus, τ_s is the time from arrival on the destination torus to the appropriate invariant curve, then, $\theta_{1,u}$ and $\theta_{1,s}$ are the latitudinal angles along the invariant curve for the initial and destination tori, respectively. The Jacobian for the targeting problem is subsequently defined,

$$\mathbf{DF} = \begin{bmatrix} I_{6\times 6} & 0_{6\times 1} & \frac{\partial \boldsymbol{F}_1}{\partial \tau_u} & 0_{6\times 1} & \frac{\partial \boldsymbol{F}_1}{\partial \theta_{1,u}} & 0_{6\times 1} \\ \Phi(T_T, 0) & \dot{\boldsymbol{x}}_T^t & 0_{6\times 1} & \frac{\partial \boldsymbol{F}_2}{\partial \tau_s} & 0_{6\times 1} & \frac{\partial \boldsymbol{F}_2}{\partial \theta_{1,s}} \end{bmatrix} \tag{6}$$

where $\boldsymbol{\Phi}(T_T, 0)$ is the state transition matrix from $\boldsymbol{x}_T$ to $\boldsymbol{x}_T^t$ and $\dot{\boldsymbol{x}}_T^t$ is the time derivative of $\boldsymbol{x}_T^t$. The derivative of the unstable manifold constraint with respect to τ_u is defined,

$$\frac{\partial \boldsymbol{F}_1}{\partial \tau_u} = -\dot{\boldsymbol{x}}_{M,u} - d_u \left(\frac{\dot{\Phi}_u \boldsymbol{v}_u}{(\boldsymbol{v}_u^T \Phi_u^T \Phi_u \boldsymbol{v}_u)^{\frac{1}{2}}} - \Phi_u \boldsymbol{v}_u \frac{\boldsymbol{v}_u^T \Phi_u^T \dot{\Phi}_u \boldsymbol{v}_u + \boldsymbol{v}_u^T \dot{\Phi}_u^T \Phi_u \boldsymbol{v}_u}{2(\boldsymbol{v}_u^T \Phi_u^T \Phi_u \boldsymbol{v}_u)^{\frac{3}{2}}} \right) \tag{7}$$

where $\dot{\boldsymbol{\Phi}}_u$ is the time derivative of the state transition matrix evaluated at $\boldsymbol{x}_{M,u}^t$. The state transition matrix is the gradient of the state equations for the CR3BP, defined in Eq. (1). The derivative of the stable manifold constraint with respect to τ_s is developed similarly. The derivative of the unstable manifold constraint with respect to $\theta_{1,u}$ is subsequently defined,

$$\frac{\partial \boldsymbol{F}_1}{\partial \theta_{1,u}} = -\Phi_u \frac{\partial \boldsymbol{x}_{M,u}}{\partial \theta_{1,u}} - d_u \frac{\partial \left(\Phi \boldsymbol{v}_u (\boldsymbol{v}_u^T \Phi^T \Phi \boldsymbol{v}_u)^{-\frac{1}{2}} \right)}{\partial \theta_{1,u}} \tag{8}$$

where $\frac{\partial \boldsymbol{x}_{M,u}}{\partial \theta_1}$ is summarized by McCarthy [21]. The second term on the right side in Eq. (8) defined is evaluated as,

$$\frac{\partial \left(\Phi_u \boldsymbol{v}_u (\boldsymbol{v}_u^T \Phi_u^T \Phi_u \boldsymbol{v}_u)^{-\frac{1}{2}} \right)}{\partial \theta_{1,u}} = \frac{\frac{\partial \Phi_u}{\partial \theta_{1,u}} \boldsymbol{v}_u + \Phi_u \frac{\partial \boldsymbol{v}_u}{\partial \theta_{1,u}}}{\left(\boldsymbol{v}_u^T \Phi_u^T \Phi_u \boldsymbol{v}_u \right)^{\frac{1}{2}}} - \Phi_u \boldsymbol{v}_u M \tag{9}$$

where $\mathbf{M}$ is defined,

$$\mathbf{M} = \frac{\frac{\partial \boldsymbol{v}_u}{\partial \theta_{1,u}}^T \boldsymbol{\Phi}_u^T \boldsymbol{\Phi}_u \boldsymbol{v}_u + \boldsymbol{v}_u^T \frac{\partial \boldsymbol{\Phi}_u}{\partial \theta_{1,u}}^T \boldsymbol{\Phi}_u \boldsymbol{v}_u + \boldsymbol{v}_u^T \boldsymbol{\Phi}_u^T \frac{\partial \boldsymbol{\Phi}_u}{\partial \theta_{1,u}} \boldsymbol{v}_u + \boldsymbol{v}_u^T \boldsymbol{\Phi}_u^T \boldsymbol{\Phi}_u \frac{\partial \boldsymbol{v}_u}{\partial \theta_{1,u}}}{2\left(\boldsymbol{v}_u^T \boldsymbol{\Phi}_u^T \boldsymbol{\Phi}_u \boldsymbol{v}_u\right)^{\frac{3}{2}}} \tag{10}$$

and the term $\frac{\partial \boldsymbol{\Phi}_u}{\partial \theta_{1,u}}$ is evaluated numerically via 4th order finite differencing [22]. Numerical experiments demonstrate that leveraging higher-order finite differencing to compute $\frac{\partial \boldsymbol{\Phi}_u}{\partial \theta_{1,u}}$ improves the convergence behavior of the differential corrections process. The term $\frac{\partial \boldsymbol{v}_u}{\partial \theta_{1,u}}$ is defined using a Fourier series expansion to represent the unstable eigenvector directions along the invariant curve,

$$\frac{\partial \boldsymbol{v}}{\partial \theta_1} = \mathrm{i} e^{\mathrm{i}\theta_1 \boldsymbol{k}} \mathrm{diag}[\boldsymbol{k}] \mathbf{C}_u \tag{11}$$

where $\mathbf{C}_u$ is the matrix of Fourier coefficients that is constructed from the unstable eigenvector directions on the invariant curve. To compute the matrix $\mathbf{C}_u$, the unstable eigenvectors associated with the discrete states along the invariant curve are rearranged into an $N \times 6$ matrix, $\mathbf{V}_u$, such that the i^{th} row represents the unstable eigenvector direction for the i^{th} state along the invariant curve,

$$\mathbf{C}_u = \mathbf{D}\mathbf{V}_u \tag{12}$$

with $\mathbf{D}$ as the discrete Fourier transform, as defined by McCarthy and Howell [14]. The partial derivatives of the stable manifold constraint with respect to the latitudinal angle on the arrival orbit is constructed similarly. Note that there is one more constraint than free variable for this problem formulation. However, since the Jacobi Constant is implicitly constrained when solving for a heteroclinic connection in the CR3BP, one of the state constraints is removed. Furthermore, a sign ambiguity exists when one of the state constraints is removed. To ensure that 6-element state is continuous between $\boldsymbol{x}_T^t$ and $\boldsymbol{x}_{M,s}^t$ when the differential corrections process has completeled, the $\dot{y}$ component of the state is removed from the continuity constraint. Note that if the element that is removed is near zero, then the differential corrections process can converge to a solution that does not possess 6-element state continuity due to the sign ambiguity. Subsequently, there are 11 constraints and 11 free variables and a unique solution between two quasi-periodic orbits at the same value of Jacobi Constant, given such a connection exists. This formulation is also extendable to a multiple-shooting problem, where the transfer segment is decomposed into smaller segments. Even though the number of constraints is equal to the number of free variables, there is no guarantee that a connection exists from a selected initial guess. First, the initial guess may not be sufficiently close to the final solution for the corrections algorithm to effectively solve for the connection or a connection simply does not exist for these exact QPOs and a solution nearby, at a slightly higher or lower Jacobi Constant, is sought. Subsequently, to aid in the convergence from the initial guess, an additional free variable can be appended to the free variable vector in Eq. (5). While the addition of this free variable does not guarantee convergence, it improves convergence behavior by adding a degree of freedom in the targeting

problem. This free variable is a parameter that characterizes the departing or destination QPO such the departing/destination orbit is allowed to vary during the targeting process. For example, consider the appended free variable to be the rotation angle ρ_u that corresponds to the rotation angle for the departing quasi-periodic orbit. By appending ρ_u to the end of the free-variable vector, the departing QPO is recomputed using the algorithm summarized by Gomez and Mondelo as well as Olikara and Scheeres (denoted the GMOS algorithm), within each iteration of the targeting process [17]. However, challenges exist when evaluating the variations of the stable eigenvector direction with respect to ρ_u, i.e., $\frac{\partial v_u}{\partial \rho_u}$, since these variations cannot be computed analytically. The accuracy of the derivatives of the unstable eigenvector with respect to the rotation angle is related to the accuracy for which the eigenvectors are computed for the departing quasi-periodic orbit. To resolve this challenge, the ρ_u free variable is included until the constraint vector reaches a tolerance of 0.0000001, then ρ_u is removed from the free variable vector. This strategy attempts to relax the sensitivity of the problem such that an initial basin of convergence is accessed. To demonstrate the process, the initial guess from the map in Fig. 3 is supplied to the differential corrections procedure and the resulting converged heteroclinic connection is rendered in Fig. 5a.

4.4 Families of Heteroclinic Connections

Given that this targeting problem produces a unique transfer solution, the process is extended to construct families of heteroclinic transfers. To construct families, a parameter to represent the destination orbit is included in the process. Since quasi-periodic orbits are uniquely defined by two parameters in the CR3BP and the Jacobi Constant is constrained between the initial and final orbits, the rotation angle is selected as the parameter to characterize the destination orbit within a family of heteroclinic connections. The initial converged transfer from Fig. 5a seeds a natural

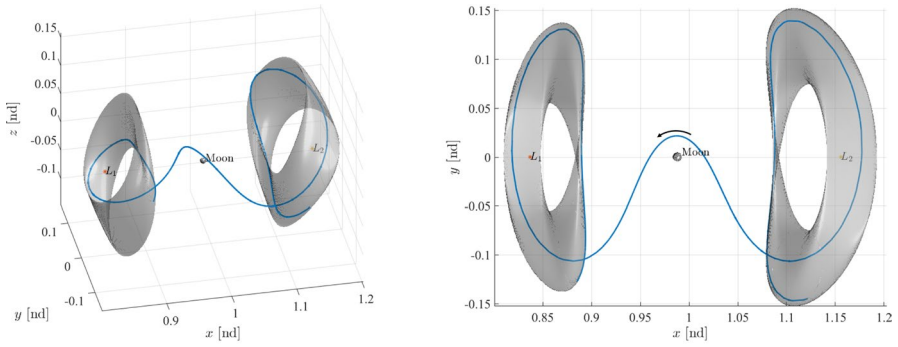

Fig. 5 **a** Converged heteroclinic connection between the two quasi-halo orbits with $JC = 3.11$. **b** $\hat{x}\hat{y}$ projection of the converged heteroclinic transfer. Arrows indicate the the direction of motion

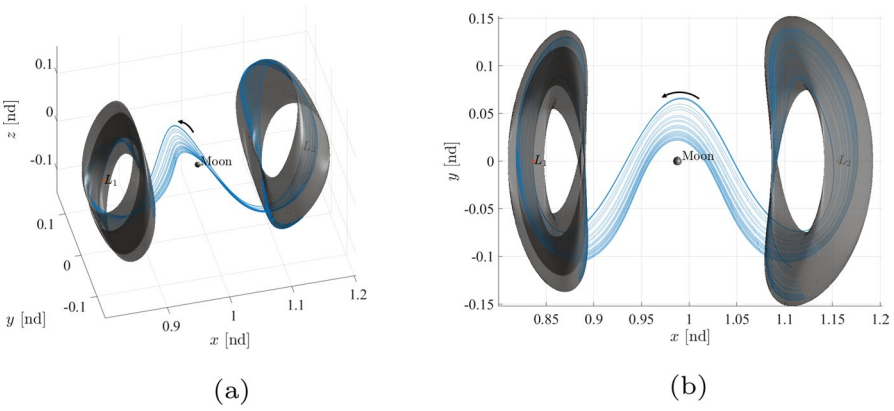

Fig. 6 Family of heteroclinic transfers between an L_2 quasi-halo orbit with $\rho = 0.48882741$ and a range of L_1 quasi-halo orbits with $JC = 3.11$. Arrows indicate the direction of motion. The first and last L_1 quasi-halo orbits from the family are plotted in each projection

parameter continuation process, where the destination orbit, characterized by the rotation angle, ρ_s, is modified for each member of the family. The parameter ρ_s is considered as the continuation parameter when generating the family of transfers. Subsequently, the value of ρ_s is incremented by 0.01 to seed the next member of the family. Members of the family of heteroclinic transfers where $JC = 3.11$ are rendered in Fig. 6a. Note that the gaps in the continuum of transfer solutions occur where the ratio of the latitudinal and longitudinal frequencies associated with the departing orbit is very near or equal to an integer ratio. Similarly, using the same initially converged transfer solution in Fig. 5a, a family of heterclinic connections is

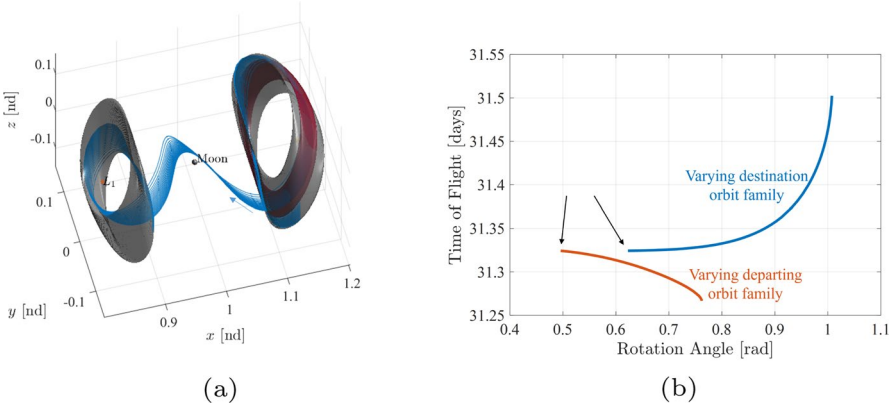

Fig. 7 **a** Family of heteroclinic transfers between a range of L_2 quasi-halo orbits with $JC = 3.11$ and an L_1 quasi-halo orbit with $\rho = 0.6226313$. Arrows indicate the direction of motion. The first and last L_2 quasi-halo orbits from the family are plotted in each projection. **b** Time-of-flight as a function of the rotation angle for the departing/destination orbits. The blue curve corresponds to the family in Fig. 6a and the orange curve corresponds to the family in 7a

constructed such that the departing L_2 quasi-halo orbit is modified for each member of the family. The family is rendered in Fig. 7a. In Fig. 7b, time-of-flight is plotted as a function of the rotation angle of the orbit that is varying across the family, i.e., the blue curve corresponds to the time-of-flight associated with the transfers rendered in Fig. 6a as a function of the destination orbit rotation angle and the orange curve corresponds to the time-of-flight for the transfers rendered in Fig. 7a as a function of the departing orbit's rotation angle. Note that the two curves plotted in Fig. 7b possess a common time-of-flight equal to 31.325 days, at the location indicated by the black arrows. The common time-of-flight corresponds to the initially converged solution from Fig. 5a. This same methodology is employed for a different destination orbit, as illustrated in Fig. 8a. The destination orbit is shifted to an L_1 quasi-vertical orbit and a family of heteroclinic transfers from L_2 quasi-halo orbits to a set of L_1 quasi-vertical orbits is successfully accomplished. Each of the transfers in Fig. 8a are colored consistent with to their times-of-flight.

Families of transfer solutions are also constructed by switching the continuation parameter. As an alternative strategy, the rotation angles for the departure destination orbits are maintained as constant, and the Jacobi Constant is then employed as the continuation parameter. Thus, each transfer in the family possesses a different departure and arrival orbit, and the Jacobi Constant varies across members of the family. During the continuation process, the L_1 and L_2 orbits are first reconverged at each continuation step such that they possess the same Jacobi Constant value. Then, the heteroclinic transfer is converged between these two orbits. To demonstrate this classification of heteroclinic transfer families, consider a transfer scenario from an L_2 quasi-vertical orbit to an L_1 quasi-vertical orbit. After selecting an initial guess, a subset of the family of heteroclinic transfers is constructed and rendered in Fig. 9a. Each transfer is colored by its Jacobi Constant value. The red surfaces represent quasi-vertical orbits with $JC = 3.15$ and the grey surfaces represent orbits with the value $JC = 3.1363$. Using Jacobi Constant as the continuation variable illuminates

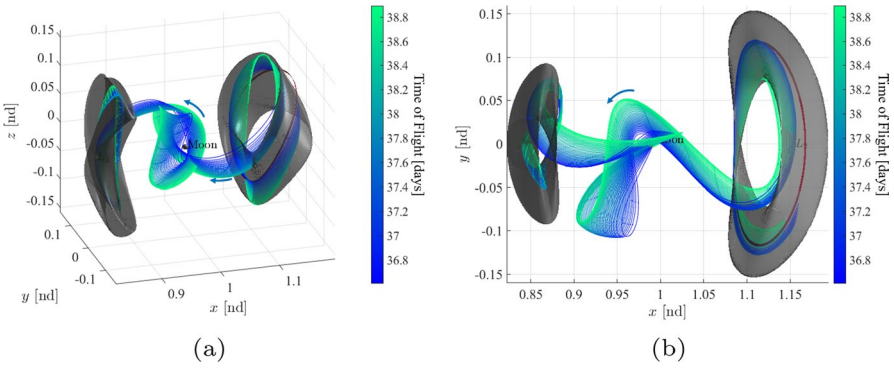

Fig. 8 Family of heteroclinic transfers between a set of L_2 quasi-halo orbits and an L_1 quasi-vertical orbit with $JC = 3.11$. Blue arrows indicate the direction of motion. The first and last L_2 quasi-vertical orbit from the family are plotted in grey and red, respectively. Each of the transfers are colored by time-of-flight

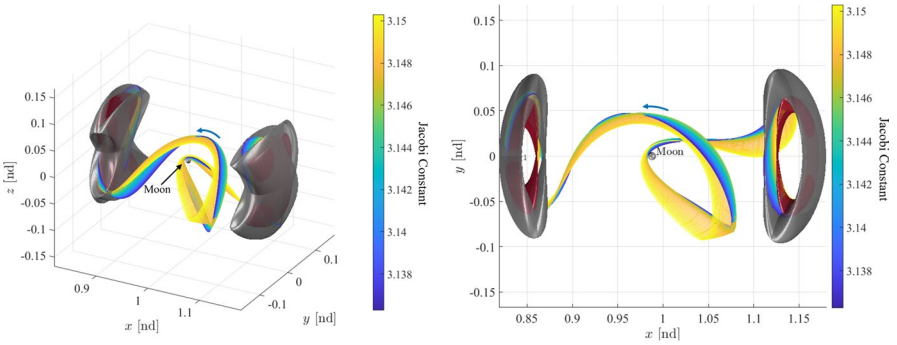

Fig. 9 Family of heteroclinic transfers between L_2 quasi-halo orbits and L_1 quasi-vertical orbits. Blue arrows indicate the direction of motion. The red surfaces represent the orbits with the highest Jacobi Constant values and the grey surfaces represent the orbits with the lowest Jacobi Constant values

alternative types of motion within the vicinity of the Moon to access the L_1 region from L_2 orbits.

Note that this investigation only leverages a natural parameter continuation process to seed each member of the family for the differential corrections process. More sophisticated continatuion methods exist, such as pseudo-arclength continuation; however, challenges exist when implementing a pseudo-arclength continuation process for this problem. The variations in the stable and unstable eigenvectors with respect to the rotation angle of the quasi-periodic orbit (i.e., the parameter representing the departing/destination orbit in the CR3BP) are not readily available analytically. Based on numerical experiments, the accuracy of the finite difference partial derivatives with respect to the rotation angle are particularly sensitive to the perturbation size. Thus, it is challenging to converge on a transfer such that the nullspace of the Jacobian is computed to sufficient accuracy to successfully construct the pseudo-arclength constraint.

Additionally, the accuracy of the partial derivatives with respect to rotation angle is related to the accuracy of the eigenvectors that are evaluated for the departing/destination quasi-periodic orbit. Since the stable and unstable eigenvectors are a function of the converged quasi-periodic orbit, the quasi-periodic orbit construction must be decoupled from the heteroclinic transfer targeting scheme. Subsequently, the rotation angle representing the departing orbit is included as a free variable and aids in the computation of a heteroclinic connection, but the non-zero columns of the Jacobian matrix that correspond to the variations with respect to the rotation angle must be computed numerically a using finite differencing method. The computation of these variations proves to be more accurate and the targeting process demonstrates improved convergence behavior when a higher-order central differencing method is used [22].

5 Ephemeris Transition

The CR3BP offers insight into the dynamical behavior associated with low-energy transfers in the Earth-Moon neighborhood; however, validation in a higher-fidelity ephemeris model is important for the design process. The ephemeris propagation and the differential corrections algorithm is implemented using the FreeFlyer™commerical off-the-shelf software package, as well as the trajectory visualization from the ephemeris model [23]. The corrections process is formulated as a two-level targeting process to produce position and velocity continuity between trajectory segments [24, 25]. The segments were generated by first discretizing the CR3BP trajectory into a set of nodes or patch points. Each node respresents a 6-element state vector along the CR3BP trajectory. Next, each node is transformed from the barycentered Earth-Moon rotating frame to the Moon-centered J2000 inertial frame using the transformation summarized by Ocampo [26]. The times-of-flight associated with each trajectory segment are equal to the difference between the time at the current node and the time at the next node. To demonstrate the existence of the heteroclinic transfer solutions in the higher-fidelity model, initial guesses from Fig. 6a and Fig. 8a are constructed to seed the ephemeris corrections process, using an initial epoch of Jan 01 2025 00:00:00.000. The quasi-halo to quasi-halo transfer is associated with an initial guess in the CR3BP that possesses a 31.43 day time-of-flight and the quasi-halo to quasi-vertical transfer initial guess is associated with the CR3BP solution that possesses a 38.55 day time-of-flight. To ensure that the geometry of the departure and destination orbits are maintained, the initial guess is constructed to include 200 days of a path along the departure orbit and 200 days of a path along the destination orbit. The transfers are converged in the Sun-Earth-Moon point-mass ephemeris model and rendered in Fig. 10. Note that the geometry characteristics are maintained after the transition to the ephemeris model and no maneuver is required to transfer between each of these orbits, i.e., each transfer is entirely ballistic. With this transfer converged in the ephemeris model, further analysis can be performed or the trajectory can be adjusted in response to any specific requirements.

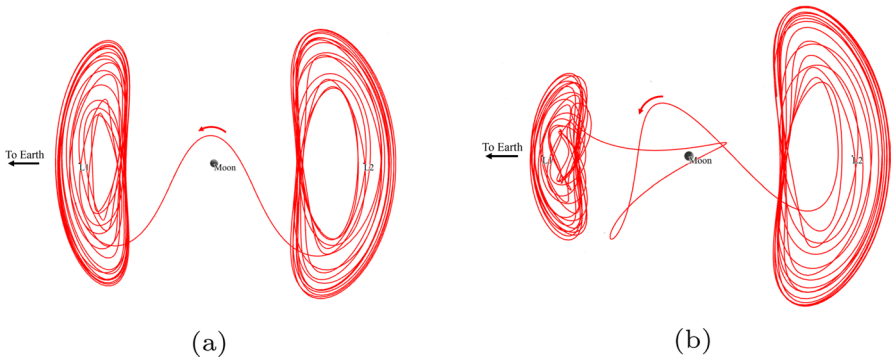

Fig. 10 Two heteroclinic transfers converged in a Sun-Earth-Moon ephemeris model and rendered in FreeFlyer the Moon-centered, Earth-Moon rotating frame. The red arrows indicate the direction of motion

Lastly, the initial guesses provided to the transition process in this investigation are not depenedent on epoch when transitioning to an ephemeris model. However, when considering initial guesses constructed in a time-dependent model, such as the Bicircular Restricted Four-Body Problem (BCR4BP) or the Elliptic Restricted Three-Body Problem (ER3BP), the epoch provided to the differential corrections alogrithm must be selected based on information from the model in which the initial guess was constructed. Such a process has been previously been demonsrated by McCarthy and Howell [20] as well as Park and Howell [27].

6 Concluding Remarks

Quasi-periodic orbits expand the range of accessible fundamental motions and add flexibility for trajectory design. For unstable quasi-periodic orbits, manifold structures are leveraged to supply transfer options into destination orbits in the vicinity of the Earth and Moon. These strategies are also effective for other three-body systems. Poincaré mapping techniques are leveraged to isolate possible heteroclinic connections and produce an initial guess to generate families of heteroclinic transfers. Lastly, transition to an ephemeris model is accomplished using a two-level targeting process to ensure that these solutions exist in a higher-fidelity model. The properties of the fundamental behaviors serve as the basis for a wider array of options in preliminary path planning.

Acknowledgements The authors thank the Purdue University School of Aeronautics and Astronautics, as well as the Rune and Barbara Eliasen Visualization Laboratory for facilities and financial support. The authors also thank a.i. solutions, Inc. for financial support and technical support to produce the ephemeris results in this paper. Lastly, the authors recognize and appreciate valueable discussions with Dr. Kenza Boudad, Stephen Scheuerle, Rolfe Power, and the rest of the members of Purdue's Multi-Body Dynamics Research Group for insight concerning this investigation.

References

1. National Aeronautics and Space Administration: NASA's Lunar Exploration Program Overview. NP-2020-05-2853-HQ (2020)
2. Hambleton, K., Fairley, T., Cheshier, L.: Splashdown! NASA's Orion Returns to Earth After Historic Moon Mission. web (2022). https://www.nasa.gov/press-release/splashdown-nasa-s-orion-returns-to-earth-after-historic-moon-mission
3. Calleja, R.C., Doedel, E.J., Humphries, A.R., Lemus-Rodriquez, A., Oldeman, B.E.: Boundary value problem formulations for computing invariant manifolds and connecting orbits in the circular restricted three body problem. Celest. Mech. Dyn. Astron. **114**(1–2), 77–106 (2012)
4. Gómez, G., Koon, W.S., Lo, M.W., Marsden, J.E., Masdemont, J., Ross, S.D.: Connecting orbits and invariant manifolds in the spatial restricted three-body problem. Nonlinearity **17**(5), 1571–1606 (2004)
5. Olikara, Z.: Computation of Quasi-Periodic Tori and Heteroclinic Connections in Astrodynamics Using Collocation Techniques. Ph.D. Dissertation, University of Colorado, Boulder, Boulder, Colorado (January 2016)

6. Bonasera, S., Bosanac, N.: Transitions Between Quasi-Periodic Orbits Near Resonances in the Circular Restricted Three-Body Problem. In: AAS/AIAA Astrodynamics Specialist Virtual Conference, Lake Tahoe, California (2020)
7. Smet, S.D., Scheeres, D.J.: Identifying heteroclinic connections using artificial neural networks. Acta Astronautica **161**, 192–199 (2019)
8. Henry, D., Scheeres, D.: A Survey of Heteroclinic Connections in the Earth-Moon System. In: 73rd International Astronautical Congress, Paris, France (2022)
9. McCarthy, B., Howell, K.: Accessing the Vicinity of the L1 Libration Point Via Low-Energy Transfers Leveraging Quasi-Periodic Orbits. In: AAS/AIAA Astrodynamics Specialist Conference, Charlotte, North Carolina (2022)
10. Szebehely, V.: The Theory of Orbits: The Restricted Problem of Three Bodies. Academic Press Inc, New York (1967)
11. Cox, A.D., Bosanac, N., Guzzetti, D., Howell, K., Folta, D.C., Webster, C.M.: An Interactive Trajectory Design Environment Leveraging Dynamical Structures in Multi-Body Regimes. In: 6th International Conference on Astrodynamics Tools and Techniques, Darmstadt, Germany (2016)
12. Folta, D.C., Webster, C.M., Bosanac, N., Cox, A.D., Guzzetti, D., Howell, K.C.: Trajectory Design Tools for Libration and Cislunar Environments. In: International Conference on Astrodynamics Tools and Techniques, Darmstadt, Germany (2016)
13. Olikara, Z.P., Scheeres, D.J.: Numerical Methods for Computing Quasi-Periodic Orbits and Their Stability in the Circular Restricted Three-Body Problem. In: IAA Conference on Dynamics and Control of Space Systems, Porto, Portugal (2012)
14. McCarthy, B.P., Howell, K.C.: Leveraging quasi-periodic orbits for trajectory design in cislunar space. Astrodynamics **5**(2), 139–165 (2021)
15. Gomez, G., Mondelo, J.M.: The dynamics around the collinear equilibrium points of the RTBP. Phys. D: Nonlinear Phenom. **157**(4), 283–321 (2001)
16. Castella, E., Jorba, A.: On the vertical families of two-dimensional tori near the triangular points of the bicircular problem. Celest. Mech. Dyn. Astron. **76**, 35–54 (2000)
17. Baresi, N., Olikara, Z.P., Scheeres, D.J.: Fully numerical methods for continuing families of quasi-periodic invariant tori in astrodynamics. J. Astronaut. Sci. **65**(2), 157–82 (2018)
18. Jorba, A.: Numerical computation of the normal behavior of invariant curves of n-dimensional maps. Nonlinearity **14**(5), 943–976 (2001)
19. Haapala, A., Howell, K.C.: A framework for construction of transfers linking Periodic libration point orbits in the earth-moon spatial circular restricted three-body problem. J. Bifurc. Chaos **26**(5), 1630013–1163001340 (2016)
20. McCarthy, B., Howell, K.: Four-body cislunar quasi-periodic orbits and their application to ballistic lunar transfer design. Adv. Space Res. **71**(1), 556–84 (2023)
21. McCarthy, B.P.: Cislunar Trajectory Design Methodologies Incorporating Quasi-Periodic Structures with Applications. PhD Dissertation, Purdue University, West Lafayette, Indiana (May 2022)
22. Fornberg, B.: Generation of finite difference formulas on arbitrarily spaced grids. Math. Comput. **51**(184), 699–706 (1988)
23. a.i. solutions: Freeflyer Version 7.8.0. a.i. solutions, Inc
24. Marchand, B., Howell, K., Wilson, R.: Improved corrections process for constrained trajectory design in the n-body problem. J. Spacecr. Rockets **44**, 884–897 (2007)
25. McCarthy, B.: Two-Level Targeter for Transforming from CR3BP. In: Freeflyer Users Conference 2020, Virtual (2020)
26. Ocampo, C.A.: An Architecture for a Generalized Trajectory Design and Optimization System. In: International Conference on Libration Points and Missions, Aiguablava, Spain (2002)
27. Park, B., Howell, K.: Leveraging Intermediate Dynamical Models for Transitioning from the Circular Restricted Three-Body Problem to an Ephemeris Model. In: AAS/AIAA Astrodynamics Specialist Conference, Charlotte, North Carolina (2022)